MOL #50773

Different interactions between MT7 toxin and the human muscarinic M_1 receptor in its free and NMS-occupied states

Carole Fruchart-Gaillard, Gilles Mourier, Catherine Marquer, Enrico Stura,

Nigel J. M. Birdsall and Denis Servent

CEA, iBiTecS, Service d'Ingénierie Moléculaire des Protéines (SIMOPRO), Laboratoire de Toxinologie Moléculaire et Biotechnologie, Gif sur Yvette, F-91191, France.(C.F-G, G. M., C. M., E. S., D. S.) and Division of Physical Biochemistry, MRC National Institute for Medical Research, Mill Hill, London, UK (N.J.M.B).

1

MOL #50773

Running title:

MT7 interactions with free and occupied hM$_1$ receptors

Corresponding author : D. Servent CEA, iBiTecS, Service d'Ingénierie Moléculaire des Protéines (SIMOPRO), Laboratoire de Toxinologie Moléculaire et Biotechnologie, Gif sur Yvette, F-91191, France. Tel : 33 1 69 08 52 02, Fax : 33 1 69 08 90 71. E-mail: denis.servent@cea.fr

Number of text pages: 24

Number of tables: 3

Number of figures: 7

Number of references: 33

Number of words in abstract: 248

Number of words in Introduction: 728

Number of words in Discussion: 1644

Abbreviations : MT7, muscarinic toxin 7; NMS, N-methylscopolamine; DMF, dimethylformamide; TFA, trifluoroacetic acid; PBS, phosphate buffered saline; BSA, bovine serum albumin; CD, circular dichroism; CCh, carbamylcholine, carbachol; ACh, acetylcholine; hM$_1$, human M$_1$ muscarinic receptor subtype; AChBP, ACh binding protein from *Aplysia*

Abstract

Muscarinic MT7 toxin is a highly selective and potent antagonist of the M_1 subtype of muscarinic receptor and acts by binding to an allosteric site. To identify the determinants by which this toxin interacts with this receptor in its free and NMS-occupied states, the effect of alanine-substitution of the toxin on its potency was evaluated in equilibrium and kinetic binding experiments as well as in functional assays. The determination of the crystallographic structure of an MT7-derivative (MT7-diiodoTyr51) allowed the selection of candidate residues which are accessible and present on both faces of the three toxin loops. The equilibrium binding data are consistent with negative cooperativity between NMS and wild-type or modified MT7 and highlight the critical role of the tip of the central loop of the toxin (Arg34, Met35 Tyr36) in its interaction with the unoccupied receptor. Examination of the potency of wild-type and modified toxins to allosterically decrease the dissociation rate of [^{3}H]NMS allowed the identification of the MT7 residues involved in its interaction with the NMS-occupied receptor. In contrast to the results with the unoccupied receptor, the most important residue for this interaction was Tyr36 in loop II, assisted by Trp10 in loop I and Arg52 in loop III. The critical role of the tips of the MT7 loops was also confirmed in functional experiments. The high specificity of the MT7-M_1 receptor interaction exploits several MT7-specific residues and reveals a different mode of interaction of the toxin with the free and NMS-occupied states of the receptor.

MOL #50773

Muscarinic neurotoxins, small peptides of 64-66 residues derived from the venom of African mambas (*Dendroaspis angusticeps* and *Dendroaspis polylepis*), are well known for their ability to interact with different muscarinic receptor subtypes. NMR and X-ray studies of the MT2 toxin have shown that muscarinic toxins have the three-finger fold structure, characteristic of the large superfamily of toxins that act at cholinergic synapses (Ménez and Ducruix, 1993 ; Ségalas et al., 1995; Servent and Ménez, 2001). Ten different muscarinic toxins have been isolated so far. Despite their high sequence homology, they show divergent interaction profiles with the different muscarinic receptor subtypes, (reviewed in (Bradley, 2000; Karlsson et al., 2000)). For instance the MT7 toxin, purified from the venom of the green mamba, binds to the M_1 receptor subtype with a potency in the low or sub-nanomolar range, with at least 10,000-fold selectivity relative to the other receptor subtypes (Carsi and Potter, 2000; Max et al., 1993; Mourier et al., 2003; Olianas et al., 2000). Pharmacological and functional studies of the MT7-hM$_1$ interaction have demonstrated that it (i) inhibits ACh-stimulated [^{35}S]GTPγS binding to CHO cell membranes expressing M_1 receptors, (ii) dissociates very slowly from M_1 receptors and (iii) strongly decreases or increases the rate of dissociation of [^{3}H]NMS and [^{3}H]ACh, respectively (Krajewski et al., 2001; Mourier et al., 2003 ; Olianas et al., 2004; Olianas et al., 2000). In summary, MT7 acts as a highly selective antagonist of M_1 receptors by establishing a strong and stable interaction with an allosteric binding site on the receptor.

There is a limited understanding of the specificity, selectivity and mechanism of action of the muscarinic toxins at muscarinic receptor subtypes and the location of the binding sites used by the toxins has proved to be quite challenging. Because of its high affinity and highest subtype selectivity several studies have investigated the MT7-human M_1 receptor (hM$_1$) interaction using wild-type and modified muscarinic toxins. Expression of recombinant MT7 in the baculovirus vector-Sf9 insect cell system (Nasman et al., 2000) and in *Pichia pastoris* (Krajewski et al., 2001) has resulted in relatively low yields. However, using a one-step solid-phase chemical synthesis, we have been able to achieve good yields of muscarinic toxins (Fruchart-Gaillard et al., 2006; Mourier et al., 2003) and have shown that synthetic MT1 and MT7 toxins possess physicochemical and pharmacological profiles identical to those of purified natural toxins. Furthermore, we have been able to demonstrate that the two toxins appear to recognize the hM$_1$ receptor differently (Mourier et al., 2003).

Like other members of family A of G-protein coupled receptors, the hM_1 muscarinic receptor is characterized by its having at least two distinct binding sites. Agonists and competitive antagonists bind to the orthosteric site, located inside the transmembrane domain, whereas allosteric agents induce a significant perturbation of the kinetics of binding of ligands to the primary site by interacting with an allosteric site, located more extracellularly (Christopoulos and Kenakin, 2002; Christopoulos et al., 1998 ; Ellis et al., 1993; Stockton et al., 1983, Matsui et al., 1995). The effects of allosteric ligands, such as the MT7 toxin, are consistent with a ternary complex model in which the orthosteric and allosteric agents can bind simultaneously to the receptor and modify each other's affinity (Ehlert, 1988 ; Lazareno and Birdsall, 1995). Recently, we have characterized directly and indirectly, using equilibrium and kinetic experiments, the MT7 affinity for the free and NMS-occupied receptor, using an iodinated MT7 derivative and [^{3}H]NMS, respectively (Fruchart-Gaillard et al., 2006). The similar results obtained using the two approaches confirm the reciprocity of the NMS-MT7 cooperative interaction and validate the allosteric ternary complex model used to study the MT7-hM_1 interaction.

In this paper, we have attempted to delineate the interaction sites by which the MT7 toxin recognizes the hM_1 receptor and have tried to explain the molecular origin of the high affinity and selectivity of this interaction. We first solved the crystallographic structure of a diiodo-MT7 analog which revealed particular structural properties that were considered to possibly be relevant to the unique pharmacology of MT7. This structure highlighted candidate toxin residues to be modified. Thus, we synthesized twelve MT7 variants, each with a single amino acid modification on one of the three toxin loops and analyzed the effect of these modifications on the MT7 potency for the free or NMS-occupied hM_1 receptor using equilibrium and kinetic binding experiments as well as functional assays.

Materials and Methods

Materials. [³H]N-Methylscopolamine ([³H]NMS), (78 Ci/mmol) was from PerkinElmer Life Sciences (Courtaboeuf, France). Atropine was from Sigma-Aldrich (St Quentin-Fallavier, France). Automated chain assembly was performed on a standard Applied Biosystems 433 peptide synthesizer (Applied Biosystems; Courtaboeuf, France). FLEXstation calcium assay kit (Molecular Devices Ltd, Wokingham, UK) was the calcium-specific fluorescent dye used in this study and the calcium flux measurement was done on a FLEXstation machine (Molecular Devices Ltd, Wokingham UK).

Peptide synthesis, disulfide bond formation and protein purification. Chemical synthesis, refolding and purification of the modified toxins were carried out using the methods described previously for the synthesis of the muscarinic MT1 and MT7 toxins (Mourier et al., 2003). Briefly, the toxins were synthesized using the Fmoc-stepwise solid-phase method with dicyclohexylcarbodiimide/1-hydroxy-7-azabenzotriazole as coupling reagents and N-methyl pyrrolidone as the solvent. After TFA deprotection and purification of the crude material, the reduced form of the pure modified synthetic toxins was subjected to an oxidative reaction using a mixture of reduced and oxidized glutathione in the presence of guanidine hydrochloride (0.5M). Finally, the toxins were purified by reverse phase HPLC using a Vydac C18 column (250 x 10 mm) with a gradient of 40 to 60% of solvent B in 40 min (A: 0.1% TFA in H_2O, B: 60% acetonitrile and 0.1% TFA in H_2O) and analytically characterized. Mass determinations were performed on a micromass platform II (Micromass, Altrincham, UK).

Circular dichroism analysis. CD spectra were recorded on a Jobin Yvon CD6 spectropolarimeter. Measurements were routinely performed at 20°C in 0.1 cm path length quartz cells (Hellma) with a peptide concentration of 5.10^{-6} M in 5 mM sodium phosphate buffer pH 7.4. Spectra were recorded over the 186 to 260 nm wavelength range. Each spectrum represents the average of four spectra.

Crystallisation and X-ray structure of MT7 derivatives. Crystals of diiodo-MT7 (labelled at Tyr51) were grown by vapour diffusion from lyophilised toxin which was re-suspended at 5 mg/ml in 50mM sodium acetate, pH 4.6. The reservoir solution used was 1.25 M ammonium sulphate, 90 mM sodium citrate, 10% methyl pentanediol, pH 5.5 with drops consisting of 1µl toxin and 1µl reservoir solution. After 6 months equilibration in a cooled

incubator at 20°C the crystals were harvested. Data to 1.38 Å resolution were collected at the ESRF beamline ID14-2 in Grenoble (France) from crystals cryo-cooled in 80% saturated Li_2SO_4 as a cryoprotectant. The HKL suite (Otwinowski and Minor, 1997) of programs was used for data reduction and the structure was solved by molecular replacement using MOLREP (CCP4; (Vagin and Teplyakov, 1997)) using the coordinates of the muscarinic toxin MT2 (PDB ID 1FF4; Ménez et al., in preparation). The XtalView suite (McRee, 1999) was used for electron density map interpretation and other graphical analysis. The structure was refined with REFMAC (Murshudov et al., 1997) to 1.42 Å and gave R-work and R-free of 20.3% and 22.1%, respectively. The PDB ID code of the diiodo-MT7 derivative is 2vlw.

CHO cells and membrane preparation. Profs. P. O. Couraud & A. D. Strosberg (ICGM, Paris, France) kindly provided CHO cells stably expressing the cloned human muscarinic M_1 – M_4 receptors and the M_5 clone was from the Guthrie cDNA resource center (www.cdna.org). The cells were grown in plastic Petri dishes (Falcon) which were incubated at 37°C in an atmosphere of 5% CO_2 and 95% humidified air in Ham F12 medium pre-complemented with L-glutamine and bicarbonate (Sigma), supplemented with 10% fetal calf serum and 1% penicillin/streptomycin (Sigma)**.** At 100% confluence, the medium was removed and the cells were harvested using a Versene buffer (PBS+5 mM EDTA). The cells were washed with ice-cold phosphate buffer and centrifuged at 1700 g for 10 min (4°C). The pellet was suspended in ice-cold buffer (1 mM EDTA, 25 mM Na phosphate, 5 mM $MgCl_2$, pH 7.4) and homogenized using an Elvhjem-Potter homogenizer (Fisher Scientific Labosi, Elancourt, France). The homogenate was centrifuged at 1700 g for 15 min (4°C). The sediment was resuspended in buffer, homogenized and centrifuged at 1700 g for 15 min (4°C). The combined supernatants were centrifuged at 35000g for 30 min (4°C) and the pellet re-suspended in the same buffer (0.1 ml/dish). The membrane preparations were aliquotted and stored at -80°C. Protein concentrations were determined by the Lowry method using bovine serum albumin as standard.

[³H]-NMS binding assays

All binding experiments were carried out at room temperature, in 10 mM sodium phosphate, pH 7.2, 135 mM NaCl, 2.5 mM KCl pH 7.4, 0.1% bovine serum albumin (PBS-BSA). The effect of various toxins on the equilibrium binding of a fixed concentration of [³H]-NMS was determined in heterologous inhibition experiments. With [³H]-NMS as tracer membranes, at a protein concentration where no more than 10% of added radioligand was bound (ca.

1500cpm), were incubated in PBS-BSA at 25 °C for 18 to 22 h, with [^{3}H]NMS (0.5 nM) and varying concentrations of toxin, in a final assay volume of 300 µl. Nonspecific binding was determined in the presence of 50 µM atropine. The reaction was stopped by addition of 3 ml of ice-cold buffer (Tris 10mM), immediately followed by filtration through Whatman GF/C glass fibre filters pre-soaked in 0.5% polyethylenimine. The filters were washed once with 3 ml ice-cold buffer (PBS), dried, and the bound radioactivity counted by liquid scintillation spectrometry. Each experiment was done at least three times.

The binding data from individual experiments (n≥3) were analyzed by nonlinear regression analysis using Kaleidagraph 4.0 (Synergy Software, Reading, PA) or GraphPad Prism 4 (GraphPad Software Inc., La Jolla, CA).

After subtraction of the nonspecific binding and normalization, competition data obtained with [^{3}H]NMS were analyzed using the allosteric ternary complex model (Ehlert, 1988). We used the following equation (Gharagozloo et al., 2002):

$$B_{LX} = B_O \times \frac{(1 + K_L \cdot [L]) \cdot (1 + \alpha \cdot (K_X \cdot [X])^{nH})}{1 + (K_X \cdot [X])^{nH} + K_L \cdot [L] \cdot (1 + \alpha \cdot (K_X \cdot [X])^{nH})} \qquad (1)$$

B_{LX} denotes the specific binding of the respective radioligand L ([^{3}H]NMS) in the presence of the cooperatively interacting agent X (allosteric agent). B_O is the binding of L in the absence of X. K_L and K_X are the affinity constants for the binding of L and X, respectively, to the unliganded receptors. α denotes the cooperativity factor for the allosteric interaction between X and L (with $\alpha > 1$, $\alpha < 1$ $\alpha = 1$, indicating positive, negative, and neutral cooperativity, respectively). n_H represents the slope factor of the binding curve of X. The value of K_L used in the data analyses was 1.10^{10} M^{-1}. Unconstrained fits for inhibition curves for R34A and Y36A had estimated slope factors less than and greater than 1, respectively. However these and all the other inhibition curves could be fitted satisfactorily with slope factors of one and the derived parameters (expressed as log values) are those given in the Tables. When the slope factors were constrained to 1, the estimates of α and K_x (and $\alpha.K_x$) were independent of whether the data were analysed using the above equation to give values of α and logK_x, or the equation recast to give values of logα and logK_x , or logK_x and log$\alpha.K_x$.

Single time-point experiments were performed to measure the inhibition of the [^{3}H]NMS dissociation by wild-type and modified toxins, assuming a mono-exponential

dissociation kinetic as previously shown for MT7 (Mourier et al., 2003). These off-rate assays have been used previously to estimate the affinity of allosteric agents for the [^{3}H]NMS-occupied receptor (Lazareno et al., 2000). A high concentration of hM$_1$ membranes (2-3 mg/ml) was incubated for 15 min with a high concentration of [^{3}H]NMS (5 nM). Then, 10µl aliquots were added to tubes that were empty or contained 1 ml of 10 µM atropine alone and with varying concentrations of toxins. Non-specific binding was measured by incubating 10 µl aliquots with 10 µM atropine and [^{3}H]NMS (5 nM). After 45 min of incubation (about 2.5 dissociation half-lives) the samples were filtered and rinsed twice. The data were transformed to rate constants using the formula:

$$koff = \ln(Bo/Bt)/t \qquad (2)$$

where Bo and Bt represent the [^{3}H]NMS bound initially and after t min of dissociation, respectively. The apparent rate constants for the dissociation of [^{3}H]-NMS were determined in the presence of each concentration of toxins (kobs) and divided by the true rate constant, ko, determined in the presence of atropine only (Gnagey et al., 1999). The resulting number, less than 1, indicates a slower dissociation of [^{3}H]NMS in the presence of the toxins, as compared to the control rate constant, (0.04 min^{-1}). The values from triplicate assays were fitted using a nonlinear regression analysis to simple inhibition curves with slope factors of 1. The -log concentration inducing a half-maximal effect on [^{3}H]NMS dissociation (logK$_{diss}$), according to the allosteric ternary complex model, is the log affinity constant of the toxin for the [^{3}H]NMS-occupied receptor.

Intracellular Calcium assays

CHO cells stably expressing hM$_1$ receptor were plated (30000 to 50000 cells/well in 100 µl) on black-walled 96-well plates (Greiner). 24h after coating, the cells were first incubated with the toxins for 75 min and then for 45 additional min with the CaKit dye resuspended in Hank Balanced Salt Solution (HBSS) buffer complemented with Hepes 20mM, at pH 7.4 (R8041, Molecular Devices Ltd, Wokingham, UK). The fluorescence was recorded using a Flexstation II plate reader (Molecular Devices Ltd, Wokingham, UK) with excitation and emission wavelengths fixed at 485 and 525 nm, respectively. Drug dilutions in assay buffer were prepared in a separate 96-well plate. Parameters for drug addition to the cell plate were preprogrammed and delivery of the agonist carbamylcholine was automated through an 8-tip head pipettor, 20sec after the beginning of the recording. Dose-response curves were constructed by measuring the fluorescence intensity after normalization to the maximal

response to carbachol, measured in the absence of toxin. All data points were measured in duplicate. The measured EC_{50} for carbachol was 24 ± 4 nM.

Results

Crystallographic structure of the diiodo-MT7 toxin derivative. Crystallization screening of the wild-type MT7 and its diiodo-Tyr51 derivative clearly showed the superiority of the modified toxin in yielding crystals suitable for high resolution structural studies. While the wild type crystals suffered from a high degree of polymorphism with the best crystals diffracting to only 3 Å, the MT7 diiodo derivative gave crystals that diffracted to atomic resolution. The high resolution structure of this derivative was considered to be more informative than a low resolution structure of the wild type, given that the addition of two iodine atoms is characterized by only a minor loss in affinity for the hM_1 receptor (data not shown). The crystallographic structure of this modified MT7 was solved by molecular replacement and refined to 1.38 Å resolution with good stereochemistry (statistics in Table 1). The lattice includes two molecules in the asymmetric unit stabilized by the diiodo-tyrosines stacking against each other (Fig. 1A), explaining the superior crystallographic quality of this derivative compared to the wild-type toxin. The overall fold conforms to that of other three finger toxins (Fig. 1B). The electron density maps are excellent for the whole structure, with only the tip of loop I, residues Ser8-Ile9-Trp10-Phe11, being less well defined than the other stretches.

Selection of the modified toxin positions. The choice of the MT7 residues to be modified was based on both the sequence alignments of the different muscarinic toxins and on the crystallographic structure of the diiodo-MT7 toxin (Fig. 1B). The twelve amino acids selected to study the functional site by which MT7 interacts with the hM_1 receptor are on the toxin surface and are mainly located at the tips of the three loops, regions previously identified as major functional determinants for other three-finger fold toxins interacting with nicotinic receptors (Fruchart-Gaillard et al., 2002; Servent and Ménez, 2001) or acetylcholinesterase (Bourne et al., 1995; Marchot et al., 1997). The selected residues are spread over the three toxin loops: Lys5, Ser8 and Trp10 and Phe11 in loop I, Tyr30, Ser32, Arg34, Met35 and Tyr36 in loop II, Lys48, Tyr 51 and Arg52 in loop III, and are located on both faces of the toxin (Fig. 1B, Table 1). In addition, these residues include those highly conserved in all the muscarinic toxin sequences (Ser8, Tyr30, Arg34 and Lys48), more variable (Tyr36), or specific to the MT7 toxin (Lys5, Trp10, Phe11, Ser32, Met35, Tyr51 and Arg52).

10

Chemical synthesis, refolding, purification and circular dichroism analyses of wild-type and modified MT7 toxins. The one-step solid phase chemical synthesis of the modified MT7 toxins was performed using a program previously developed for the synthesis of nicotinic and muscarinic toxins (Mourier et al., 2003; Mourier et al., 2000). For each modified toxin the synthesis proceeded smoothly and the final TFA cleavage yielded a crude mixture in which the main component corresponded to the reduced form of each protein. These major products constituted 30 to 40% of the total reaction mixture, as analyzed by RP-HPLC. Refolding of these toxins was performed in the presence of reduced and oxidized glutathione and 0.5M guanidine hydrochloride (Mourier et al., 2003). The final yield varied from 18 to 35% for the different toxins. The refolded modified synthetic MT7 toxins were purified to homogeneity on a C18 reversed-phase HPLC column. Finally, the purity and identity of the different toxins was confirmed by electrospray mass spectrometry. To evaluate the effect of the different single modifications on the overall structure of the MT7 toxin, we measured the CD spectra of each modified synthetic toxin and compared them to that of the native form. (Fig. 2) All derivatives displayed a typical β-sheet signature with pronounced maxima and minima at 194-196 nm and 210-216 nm, respectively. Compared to the native form, the CD spectra of some derivatives show slight variations in the intensity of the two major bands, which may reflect some local structural differences. Despite these minor deviations, the different modifications introduced on the MT7 sequence seem not to have altered the overall structure of the toxin.

Equilibrium studies of the binding of wild-type and modified MT7 toxins to the hM_1 receptor. Following our previous results on wild-type MT7 demonstrating that indirect and direct inhibition experiments, using respectively [^{3}H]NMS or [^{125}I]MT7ox, can be used to characterize the MT7-hM_1 interaction (Fruchart-Gaillard et al., 2006), the effect of the twelve modifications of the MT7 sequence was evaluated using [^{3}H]NMS as tracer. In order to avoid kinetic artifacts caused by the ability of the MT7s to inhibit [^{3}H]NMS association (and dissociation) the assays were carried out overnight to ensure that equilibrium was established. All the wild-type and modified toxins caused a concentration-dependent reduction of specific [^{3}H]NMS binding to the hM_1 receptor (illustrated for selected mutants in Fig. 3).

When analysed using the allosteric ternary complex model, the different toxins showed negative cooperativity with [^{3}H]NMS. Their affinity constants for the unoccupied receptor, (logKx), calculated as described in the Materials and Methods section, are reported in Table

2. The value for the wild-type toxin was 10.47 ± 0.04 (n=20). The single amino acid modifications, K5A, S8A, F11A, Y30A, S32A, K48A, Y51A and R52A individually induced no, or small, decreases (less than 4-fold) in the affinity of MT7 for the free hM_1 receptor, whereas weak but significant Kx decreases (6-20 fold) were associated with mutations W10A, M35A and Y36A. Finally, a major effect was observed at the tip of the central loop where the R34A modification decreased the affinity of MT7 for the hM_1 receptor approximately 200-fold (Table 2) as found previously (Mourrier et al., 2003). The effects of these modifications were confirmed by direct competition binding experiments with [^{125}I]MT7ox as tracer, where the same order of decrease in toxin affinity generated by the different modifications was observed (data not shown).

As illustrated in Figure 3 there is a residual binding of [^{3}H]NMS which is not displaceable by high concentrations of toxin. This is a characteristic of the inhibition curves of negatively cooperative allosteric ligands and represents the toxin-receptor-[^{3}H]NMS complex. The fraction of residual binding was dependent on nature of the modification to the toxin, being small for wt and R52A and larger for S32A, Y36A and R34A. All the inhibition curves were analysed according to the ternary complex model (equation details in Materials and Methods) to give estimates of the log affinities of the toxins for the [^{3}H]NMS occupied receptor (log$\alpha.K_X$) and are reported in Table 2. All the inhibition curves could be fit satisfactorily with slope factors of 1. Although the precision of the data is good (sem values generally in the 1-5% range), the values of log$\alpha.K_X$ are quite difficult to estimate accurately due the fact that, for most modified toxins, the part of the inhibition curve that determines this value is just above non-specific binding values and may be only 3-5% of the specific [^{3}H]NMS signal (see e.g. Figure 3) due to the 100-fold or greater negative cooperativity between NMS and the toxins. Where there is high negative cooperativity, small changes in the estimates of non-specific binding result in large changes in the estimates of log$\alpha.K_x$ (and their 95% confidence limits) but very small changes (<0.03 log unit) in the estimates of logK_x (data not shown).

To evaluate the potential effect of the different modifications introduced into the toxin sequence on the selectivity of the MT7-hM_1 interaction, the inhibitory potency of a high concentration of each toxin (1μM) was examined on the M_2-M_5 receptor subtypes. At this concentration, none of the modified toxins were able to displace [^{3}H]NMS from these receptor subtypes, indicating that their potencies at these subtypes were above 1 μM (data not

shown). Thus, the various modifications introduced into the MT7 sequence have no detectable effect on the large selectivity of MT7 for the hM_1 receptor.

Dissociation experiments to measure the binding of wild-type and modified MT7 toxins to the NMS-occupied hM_1 receptor. Since the formation of ternary complexes are the characteristic of allosteric interactions, we have studied the effect of wild-type and modified toxins on the kinetics of binding of $[^3H]NMS$ to the hM_1 receptor. As previously described (Gnagey et al., 1999 ; Lazareno et al., 2000 ; Mourier et al., 2003), single-time-point experiments, measuring the effect of allosteric ligands on the $[^3H]NMS$ dissociation, can be used to characterize the interaction of these allosteric agents with the NMS-occupied receptor. Thus, we studied the concentration-dependence of the effect of wild-type and modified MT7 toxins on $[^3H]NMS$ dissociation, as shown in Fig. 4. All data could be fitted satisfactorily to simple inhibition curves with slope factors of 1 and extrapolating to a kobs/ko value of zero at high toxin concentrations. The $logK_{diss}$ calculated for the wild-type toxin was 8.59 ± 0.02 (n=10). Modifications of Lys5 and Phe11 in loop I, Ser32 in loop II or Lys48 and Tyr51 in loop III only had no, or small, effects (≤ 4 fold) on $logK_{diss}$. However, 6-700 fold affinity decreases were associated with the modifications M35A, R34A, S8A, Y30A, R52A, W10A and Y36A (Table 2). Therefore, all three loops of the MT7 toxin seem to be involved in its binding to the $[^3H]NMS$-liganded receptor with critical roles for Trp10 and Tyr36 in loops I and II, respectively, as they produced the largest changes.

According to the allosteric ternary complex model, the affinity of the allosteric ligand for the NMS-occupied receptor obtained from the dissociation studies ($logK_{diss}$) should be equal to the estimate from the equilibrium data ($log\alpha.K_X$) if the two manifestations of an allosteric interaction are to have a common mechanism and explanation (Lazareno and Birdsall, 1995). The primary criteria used in this study are that these two estimates should differ by less than 3-fold or the 95% confidence limits of the two estimates should overlap. The results in Table 2 show these criteria to be satisfied for MT7 and most (8/12) of the modified toxins. However there are ≥10-fold discrepancies for W10A, Y30A, Y36A and R52A. As noted in the previous section, small changes, for example in the non-specific binding estimates, can generate large changes in the values of $log\alpha.K_X$ and their confidence limits, and the data for the four constructs then satisfy the criteria. Further possible explanations for these discrepancies are considered in the Discussion.

It is possible to calculate two estimates of the negative cooperativity from the binding data, $\log\alpha^* = \log K_{diss} - \log K_X$ and $\log\alpha^\dagger = \log\alpha.K_X - \log K_X$. These are presented in Table 2. Many of the values of log cooperativity are in the range -1.8 to -2.1, reflecting those modifications to the toxin that do not differentially affect their binding to the [^{3}H]NMS-occupied and free receptor. Both data sets show higher values of log cooperativity for S32A, R34A and M35A, illustrating a less inhibitory effect of the binding of these residues of loop II to the [^{3}H]NMS-occupied receptor, relative to the free receptor. Logα^* shows a large effect on S8A, W10A, Y30A, Y36A and R52A showing a selective inhibitory effect of these modifications on the binding of the three loops of the toxins to the NMS occupied receptor, as measured by their effects on [^{3}H]NMS dissociation.

Functional assays. The effects of wild-type and modified toxins on the function of hM$_1$ receptors stably expressed at the surface of CHO cells was evaluated by measuring changes in the intracellular calcium concentration using a calcium fluorescent dye. First, the effect of µM concentrations of all the toxins was evaluated directly on the cells and the signal was compared to the control obtained with carbamylcholine (CCh, 300nM). As shown in Fig. 5A, neither the wild-type nor the modified MT7 toxins were able to activate the hM$_1$ receptor, demonstrating that these toxins are not agonists. Preincubation of the cells with increasing concentrations of MT7 was however able to abolish, in a dose-dependant manner, the CCh (100nM) activation of the hM$_1$ receptor, as visualized in figure 5B. The potency of MT7 was estimated to 2.2 ± 0.5 nM. Analogous experiments were performed with the modified toxins. The dose-response curves show that all these toxins were able to inhibit the CCh-induced hM$_1$ activation, but with variable potencies, as reported on Table 3 and illustrated in Figure 6. All inhibition curves were fitted to a slope factor of 1. There was evidence that the slopes of the inhibition curves for MT7 and Y36A were significantly greater than 1, but fitting all the inhibition curves with the slope factor as a variable resulted in no changes in pIC$_{50}$ greater than 0.03 log unit. Four modifications induced greater than 4-fold decreases in functional potency, varying from 5-fold for S32A to 10-, 20- and 50-fold for R52A, R34A and Y36A, respectively.

Discussion

Current evidence points to the high affinity, large subtype selectivity and allosteric nature of the interaction of the MT7 toxin with the hM$_1$ receptor (Carsi and Potter, 2000; Fruchart-Gaillard et al., 2006; Max et al., 1993; Mourier et al., 2003; Olianas et al., 2000). To better

understand how MT7 binds to the free and NMS-occupied hM_1 receptor and to progress toward the structural modeling of these interactions, we have investigated how different single amino acid modifications introduced into the MT7 sequence altered its potency, determined using both equilibrium and dissociation kinetics experiments as well as functional assays. The modified residues include amino acids present specifically in the MT7 toxin or highly conserved in all the muscarinic toxin sequences and located on both faces of the three toxin loops. The CD spectra of all the purified chemically-synthesized toxins, as compared to that of the wild-type toxin, suggested that the modifications introduced into the MT7 sequence caused little effect, if any, on the overall structure of the toxin.

The determination of the crystallographic structure of a diiodo-MT7 analogue, confirms the previous assumption that MT7 belongs to the three-finger fold structural family which includes several toxins acting at the cholinergic synapse. Loops II and III are similar to those found in nicotinic toxins, while loop I is somewhat different, being more distant from the other two loops and appearing to be unusually flexible at its extremity. The side chain of Phe11 is poorly defined, a rare occurrence for this type of residue at this resolution. The surrounding residues, also hydrophobic in nature, are similarly affected. The side chain of Ile9 is better ordered than that of Phe11 but less than that of Trp10. Loop I of MT2, another muscarinic toxin, shares such disorder, but this is not particularly unusual given its sequence: Ile9-Gly10-Gly11 (unpublished observations). Considering these two structures together, it is plausible that such an unusual feature may have a functional role in these toxins. One should also be aware that the extra stabilization offered in the crystal structure by the interaction of the diiodo-tyrosines could mask some additional flexibility of loop III both in the wild type toxin and in the diiodo analogue in solution. The lower conformational constraints of muscarinic toxins, together with the variations in sequence, may explain the broad pharmacological diversity that exists within the muscarinic toxin family.

Identification from equilibrium binding experiments of the MT7 residues involved in its interaction with the *free* hM_1 receptor highlights the crucial role of the tip of the toxin loop II (Arg34, Met35, Tyr36), with the highly conserved Arg34 being particularly important (Table 2). The high affinity and selectivity of the MT7 for the hM_1 receptor may be associated with the involvement of residues specific to this toxin, such as Trp10 and Met35, located respectively at the tips of the toxin loops I and II. The MT7 specific Lys65 residue, previously reported not to play a role in determining selective binding of this toxin (Krajewski et al.,

2001) is located in the upper part of the toxin structure, a region probably too far from the toxin interaction site to be important.

MT7 has been reported to decrease the dissociation rate of [^{3}H]NMS (Krajewski et al., 2001; Mourier et al., 2003; Olianas et al., 2000). This effect confirms the ability of this toxin to form a ternary complex with NMS and M_1 receptor, which is a hallmark of an allosteric interaction. The ability of MT7 derivatives to decrease [^{3}H]NMS dissociation allowed us to identify toxin residues involved in its binding to the allosteric site when the orthosteric site is occupied by NMS. Alanine-substitution introduced into the toxin's sequence induced up to 700-fold decreases in the toxin IC_{50diss} values (Table 2), and revealed major roles for Ser 8, Trp10, Tyr30 and Arg52, as well as Arg34, Met35 and Tyr36, in this interaction. It is interesting to note that these residues (excluding Arg34) are all specific to MT7 and may be related to its allosteric property which is not observed in the interaction of the homologous MT1 with the hM_1 receptor (Mourier et al., 2003).

The wild-type and modified MT7 toxins showed negative cooperativity with [^{3}H]NMS, as indicated by the log cooperative factors ($\log\alpha^\dagger$ in Table 2) derived from the equilibrium binding curves when analysed with the ternary complex equation. These values were similar for all the toxins (-1.6 to -2.1) with the exception of the S32A, and R34A toxins (-0.8 to -1.2). Furthermore, according to the ternary model, the affinity of the MT7 for the NMS-occupied receptor can be calculated 8.66, a value similar to the one obtained from the single-time point experiments 8.59. This agreement also occurs for most but not all of the modified toxins, notably W10A, Y30A, Y36A and R52A.

There are a number of possible explanations for the discrepancies. Some of the inherent problems of determining accurate values of $\log\alpha.K_X$ because of the high negative cooperativities between NMS and the toxins have been stated in the Results section. For two of these modified toxins, W10A and Y36A, the overall toxin binding affinities have also been strongly decreased and therefore high concentrations of toxins were required to observe the manifestations of negative cooperativity in the equilibrium or kinetic experiments. If, during the long duration equilibrium experiments, there were aggregation problems with high concentrations of some modified toxins, e.g Y36A, this could result in $\log\alpha.K_X$ being overestimated. On the other hand, if there are slow isomerisations of the toxin-receptor-NMS complex, then the values of $\log K_{diss}$ may be underestimated relative to $\log\alpha.K_X$ because of the

16

relatively short duration of the dissociation experiments. In general we feel that the effects of the toxins on [3H]NMS dissociation provide a more direct and accurate estimate of the affinities of the modified toxins for the [3H]NMS-occupied receptor.

The interaction of MT7 with the hM_1 receptor was also studied in functional assays based on the measurement of the calcium release in CHO-M_1 cells. First, the lack of agonism of the MT7 was observed by its inability to generate a signal and its antagonist property was confirmed by its concentration-dependant inhibition of the CCh activation with nanomolar potency (Figure 5, Table 3). This value is compatible with those reported for the functional characterization of MT7 by measuring the effect of MT7 on CCh-induced calcium release (Kukkonen et al., 2004), CCh-induced [3H]IPs accumulation (Olianas et al., 2000) or ACh-stimulation of the [35S]GTPγS binding (Olianas et al., 2000). The effect of alanine-substitution on MT7 pIC_{50} confirms the major role of the tip of the toxin loop II (Ser32, Arg34, Tyr36) in its inhibitory actions. The potency estimate of MT7 in this assay is about 60-fold lower than its dissociation constant found in the binding studies. This comparison is confounded by the fact that the IC50 value may be influenced by the cooperativity between CCh and the MT7 and the methodology of the functional assay, i.e use of a concentration of carbamycholine well above its EC_{50}, the fact that the equilibrium between the CCh and MT7 was probably not established during the time course of the assay due to the slow dissociation of the MT7 from the receptor (hemi-equilibrium), and the possibility of slow isomerisation of the MT7-receptor complex. Hemi-equilibrium and isomerisation may, or may not, be present in the modified toxins, especially when the binding of the toxins are substantially weaker than the wild-type toxin. Given these caveats, there is excellent agreement with the fold-change in functional potency and the fold-change in binding to the unoccupied receptor relative to wild type MT7 (< 3-fold discrepancy) for most modified toxins. Somewhat larger differences are observed for the two toxins (R34A and R52A) where the modifications induce a large change in binding affinity and potentially, as alluded to above, in their kinetic properties.

Comparison of the two binding sites to which MT7 interacts, the free and the NMS-occupied hM_1 receptor, points to a major role for the tip of the central loop of MT7 which is responsible in both cases for a major part of the interaction energy (Fig. 7A, 7B). This observation agrees with results reporting the interaction of structurally-related toxins with other cholinergic targets, such as nicotinic acetylcholine receptors (Bourne et al., 2005; Fruchart-Gaillard et al., 2002) and acetylcholinesterase (Bourne et al., 1995). Furthermore,

the fact that both interaction sites include mainly aromatic (Tyr36, Trp10, Tyr30) and positively charged residues (Arg34, Arg52), suggest that cation-π and electrostatic interactions might occur in the MT7-hM$_1$ interactions, as described previously in the Cbtx-AChBP and Fasciculin-acetylcholinesterase crystallographic structure complexes (Bourne et al., 2005; Bourne et al., 1995). The toxin interaction site on the hM$_1$ receptor might be located at the outer loops or at the beginning of the transmembrane domains of the receptor, assuming that the toxin doesn't penetrate deep inside the receptor (Kukkonen et al., 2004).

The variable energetic contribution of each residue of the MT7 loop II in its interaction with free or occupied receptor (e.g. Arg34 and Tyr36) and the fact that some MT7 residues seem specific for its interaction with only one receptor state, such as Ser8, Tyr30 and Arg52 for the NMS-occupied receptor, show that the interaction of MT7 with M$_1$ receptor is not identical in the presence or absence of NMS at the orthosteric site. Thus, it appears that the presence of NMS in the acetylcholine-binding pocket induces some conformational modifications in the receptor's transmembrane domains and extracellular regions, leading to appropriate adjustments of the MT7 location as compared to its interaction with the unoccupied receptor. Site-directed mutagenesis of receptor residues is in progress to identify the toxin's interaction site on the receptor, allowing the use of the mutant-cycle approach and construction of a structural model of the toxin-muscarinic receptor interaction. Such a model should be useful to understand better the different pharmacological and functional profiles of muscarinic toxins and in the future design of molecules with pre-determined subtype and allosteric specificities.

MOL #50773

References

Bourne Y, Talley TT, Hansen SB, Taylor P and Marchot P (2005) Crystal structure of a Cbtx-AChBP complex reveals essential interactions between snake alpha-neurotoxins and nicotinic receptors. *Embo J* **24**:1512-1522.

Bourne Y, Taylor P and Marchot P (1995) Acetylcholinesterase inhibition by fasciculin: crystal structure of the complex. *Cell* **83**:503-512.

Bradley KN (2000) Muscarinic toxins from the green mamba. *Pharmacol Ther* **85**:87-109.

Carsi JM and Potter LT (2000) m1-toxin isotoxins from the green mamba (Dendroaspis angusticeps) that selectively block m1 muscarinic receptors. *Toxicon* **38**:187-198.

Christopoulos A and Kenakin T (2002) G protein-coupled receptor allosterism and complexing. *Pharmacol Rev* **54**:323-374.

Christopoulos A, Lanzafame F and Mitchelson F (1998) Allosteric interactions at muscarinic cholinoceptors. *Clin Exp Pharmacol Physiol* **25**:185-194.

Ehlert FJ (1988) Estimation of the affinities of allosteric ligands using radioligand binding and pharmacological null methods. *Mol Pharmacol* **33**:187-194.

Ellis J, Seidenberg M and Brann MR (1993) Use of chimeric muscarinic receptors to investigate epitopes involved in allosteric interactions. *Mol Pharmacol* **44**:583-588.

Fruchart-Gaillard C, Gilquin B, Antil-Delbeke S, Le Novère N, Tamiya T, Corringer PJ, Changeux JP, Ménez A and Servent D (2002) Experimentally-based model of a complex between a snake toxin and the α7 nicotinic acetylcholine receptor. *Proc Natl Acad Sci (USA)* **99**:3216-3221.

Fruchart-Gaillard C, Mourier G, Marquer C, Menez A and Servent D (2006) Identification of various allosteric interaction sites on M1 muscarinic receptor using 125I-Met35-oxidized muscarinic toxin 7. *Mol Pharmacol* **69**:1641-1651.

Gharagozloo P, Lazareno S, Miyauchi M, Popham A and Birdsall NJM (2002) Substituted pentacyclic carbazolones as novel muscarinic allosteric agents: synthesis and structure-affinity and cooperativity relationships. *J Med Chem* **45**:1259-1274.

Gnagey AL, Seidenberg M and Ellis J (1999) Site-directed mutagenesis reveals two epitopes involved in the subtype selectivity of the allosteric interactions of gallamine at muscarinic acetylcholine receptors. *Mol Pharmacol* **56**:1245-1253.

Karlsson E, Jolkonen M, Mulugeta E, Onali P and Adem A (2000) Snake toxins with high selectivity for subtypes of muscarinic acetylcholine receptors. *Biochimie* **82**:793-806.

MOL #50773

Krajewski JL, Dickerson IM and Potter LT (2001) Site-directed mutagenesis of m1-toxin1: two amino acids responsible for stable toxin binding to M(1) muscarinic receptors. *Mol Pharmacol* **60**:725-731.

Kukkonen A, Perakyla M, Akerman KE and Nasman J (2004) Muscarinic toxin 7 selectivity is dictated by extracellular receptor loops. *J Biol Chem* **279**:50923-50929.

Lazareno S and Birdsall NJM (1995) Detection, quantitation, and verification of allosteric interactions of agents with labeled and unlabeled ligands at G protein-coupled receptors: interactions of strychnine and acetylcholine at muscarinic receptors. *Mol Pharmacol* **48**:362-378.

Lazareno S, Popham A and Birdsall NJM (2000) Allosteric interactions of staurosporine and other indolocarbazoles with N-[methyl-(3)H]scopolamine and acetylcholine at muscarinic receptor subtypes: identification of a second allosteric site. *Mol Pharmacol* **58**:194-207.

Marchot P, Prowse CN, Kanter J, Camp S, Ackermann EJ, Radic Z, Bougis PE and Taylor P (1997) Expression and activity of mutants of fasciculin, a peptidic acetylcholinesterase inhibitor from mamba venom. *J Biol Chem* **272**:3502-3510.

Matsui H , Lazareno S, and Birdsall NJM (1995) Probing of the location of the allosteric site on m1 muscarinic receptors by site-directed mutagenesis. *Mol Pharmacol.* **47**:88-98.

Max SI, Liang JS and Potter LT (1993) Stable allosteric binding of m1-toxin to m1 muscarinic receptors. *Mol Pharmacol* **44**:1171-1175.

McRee DE (1999) XtalView/Xfit--A versatile program for manipulating atomic coordinates and electron density. *J Struct Biol* **125**:156-165.

Ménez R and Ducruix A (1993) A toxin that recognizes muscarinic acetylcholine receptors. Preparation and characterization of crystals suitable for structural analysis. *J Mol Biol* **232**:997-998.

Mourier G, Dutertre S, Fruchart-Gaillard C, Ménez A and Servent D (2003) Chemical synthesis of MT1 and MT7 muscarinic toxins: critical role of Arg-34 in their interaction with M1 muscarinic receptor. *Mol Pharmacol* **63**:26-35.

Mourier G, Servent D, Zinn-Justin S and Ménez A (2000) Chemical engineering of a three-fingered toxin with anti-a7 neuronal acetylcholine receptor activity. *Protein Engineering* **13**:217-225.

Murshudov GN, Vagin AA and Dodson EJ (1997) Refinement of macromolecular structures by the maximum-likelihood method. *Acta Cryst* **D53**:240-255.

Nasman J, Jolkkonen M, Ammoun S, Karlsson E and Akerman KE (2000) Recombinant expression of a selective blocker of M(1) muscarinic receptors. *Biochem Biophys Res Commun* **271**:435-439.

Olianas MC, Adem A, Karlsson E and Onali P (2004) Action of the muscarinic toxin MT7 on agonist-bound muscarinic M1 receptors. *Eur J Pharmacol* **487**:65-72.

Olianas MC, Maullu C, Adem A, Mulugeta E, Karlsson E and Onali P (2000) Inhibition of acetylcholine muscarinic M(1) receptor function by the M(1)-selective ligand muscarinic toxin 7 (MT-7). *Br J Pharmacol* **131**:447-452.

Otwinowski Z and Minor W (1997) Processing of X-ray diffraction data collected in oscillation mode. *Methods Enzymol* **276**:307-326.

Ségalas I, Roumestand C, Zinn-Justin S, Gilquin B, Ménez R, Ménez A and Toma F (1995) Solution structure of a green mamba toxin that activates muscarinic acetylcholine receptors, as studied by nuclear magnetic resonance and molecular modeling. *Biochemistry* **34**:1248-1260.

Servent D and Ménez A (2001) Snake neurotoxins that interact with nicotinic acetylcholine receptors, in *Handbook of Neurotoxicology* (Massaro EJ ed) pp 385-425, Humana Press Inc., Totowa, NJ.

Stockton JM, Birdsall NJM, Burgen ASV and Hulme EC (1983) Modification of the binding properties of muscarinic receptors by gallamine. *Mol Pharmacol* **23**:551-557.

Vagin A and Teplyakov A (1997) MOLREP: an automated program for molecular replacement. *J Appl Cryst* **30**:1022-1025.

Figure Legends

Fig. 1 Crystallographic structure of the MT7 diiodo derivative. A. The lattice includes two toxin molecules in the asymmetric unit stabilized by the diiodo-tyrosines stacking against each other. B. 3D structure of this modified MT7 refined to 1.38 Å resolution. Location of all the residues studied in this paper is indicated on the three toxin loops.

Fig. 2 Far-ultraviolet CD spectra of the wild-type and different modified toxins. The spectra were monitored in 5 mM sodium phosphate buffer pH 7.4 at 20°C at a peptide concentration of 5.10^{-6} M.

Fig. 3 Inhibition of [^{3}H]NMS binding to hM_1 receptor by wild-type and modified MT7 toxins. Binding experiments were performed by incubating membrane fractions of receptor with [^{3}H]NMS (0.5 nM) and varying concentrations of toxin at room temperature, overnight. The total specific binding in each experiment was 1500 ± 300 cpm. The results are expressed as the ratio of the specific [^{3}H]NMS binding measured with (B) or without toxin (Bo) (n=3 to 10). The curve fits were based on the ternary complex equation reported in the experimental section.

Fig. 4 Inhibition of [^{3}H]NMS dissociation by various concentrations of wild-type and modified MT7 toxins. Using the single-time-point experiment as described in Materials and Methods, the rate constants for the dissociation of [^{3}H]NMS were determined in the presence of each concentration of toxin (kobs) and divided by the rate constant in the absence of toxin, ko, determined in the presence of atropine only.

Fig. 5 Functional properties of MT7 toxin. A. Signals acquired for calcium fluorescence, using the FlexStation calcium assay kit, after the addition at 20sec of CCh (300nM) and wild-type or modified MT7 toxins (10µM) on CHO-hM_1 cells. B. MT7 inhibition of the Ca^{2+} mobilization after pretreatment of the cells with increasing concentrations (0.013 to 30 nM) of the MT7 toxin, followed by a sub-maximal concentration (100nM) of CCh.

Fig. 6 Effect of wild-type and modified MT7 toxins on the CCh-induced activation of hM_1 receptor expressed in CHO cells. Dose-response curves for MT7 toxins, expressed as the percentage of the inhibition of the calcium fluorescent signal measured after CCh (100nM) activation. All experiments were performed three times in duplicate (n=3). The inhibition curves were fitted using a slope factor of 1.

MOL #50773

Fig. 7 Comparison of the binding residues through which MT7 toxin interacts with the free (A) or NMS-occupied (B) hM$_1$ receptor. The three-dimensional structure of diiodo-MT7 is shown as a space-filling representation. Residues whose alanine-substitution caused a decrease in potency of less than 5-fold are shown in green, between 5- and 10-fold in yellow, 10- and 90-fold in orange, and higher than 90-fold in pink. The violet group shows the iodide molecules of the diiodo-Tyr51. Ser32, green in A and B, is not visible in this view.

24

MOL #50773

TABLE 1 : Statistics from crystallographic analysis of the 3D structure of the MT7 diiodo Y51-derivative.

DATA COLLECTION		
Resolution (Å)		50–1.39
Total observations		47,719
Unique reflections		26,241
Completeness(%)		89.7
Space group		$P2_1$
Unit cell parameters (Å; °)		a = 27.76, b = 56.57, c = 45.30 $\beta = 95.17$
Matthew's coefficient (V_M, Å^3/Da)		2.73
REFINEMENT		
Refinement range (Å)		45.13–1.39
Outer shell (Å)		1.42–1.39
Number of reflections		24,835 (1,434)
Total atoms refined		1,478
Number of water molecules		267
Rcryst (%)		19.9
Rfree (%)		22.5
GEOMETRY		
Bonds (Å)		0.01
Angles (°)		1.46
RAMACHANDRAN PLOT		
Residues in additional allowed regions (%)		12.5
Residues in disallowed regions (%)		0.9
Average B value	Molecule A	13.3, 15.0
(main chain, side chain Å^2)	Molecule B	13.1, 15.0

$R_{sym} = \sum_h \sum_i | I_{h,i} - I_h | / \sum_h \sum_i I_{h,i}$, where I_h is the mean intensity of the i observations of symmetry-related reflections of h.

$R = \sum | F_O - F_C | / \sum F_O$ where $F_O = F_P$, and F_C is the calculated protein structure factor from the atomic model (R_{free} was calculated using 5% of the reflections).

Rmsd in bond lengths and angles are the deviations from ideal values.

MOL #50773

TABLE 2 : Affinity constants of wild-type and modified MT7 toxins calculated from equilibrium binding experiments with [³H]-NMS using the ternary complex equation ($\log K_X$ and $\log \alpha.K_X$) and from their potency to inhibit the dissociation of [³H]-NMS ($\log K_{diss}$).

Modified MT7	loop	face	$\log K_X$	$K_{X(mod)}/K_{X(wt)}$	$\log\alpha.K_x$	$\log K_{diss}$	$K_{diss(mod)}/K_{diss(wt)}$	$\log\alpha*$	$\log\alpha^\dagger$
MT7	-	-	10.47 ± 0.04	1	8.66 ± 0.12	8.59 ± 0.02	1	-1.9	-1.8
K5A	I	concave	10.15 ± 0.08	2	8.08 ± 0.30	8.20 ± 0.05	2	-2.0	-2.1
S8A	I	concave	10.18 ± 0.05	2	8.12 ± 0.20	7.52 ± 0.08	10	-2.7	-2.1
W10A	I	concave	9.68 ± 0.11	6	7.90 ± 0.07	6.62 ± 0.07	90	-3.0	-1.8
F11A	I	convex	10.43 ± 0.11	1	8.55 ± 0.40	8.02 ± 0.04	4	-2.4	-1.9
Y30A	II	concave	10.21 ± 0.05	2	8.36 ± 0.17	7.37 ± 0.03	20	-2.8	-1.9
S32A	II	concave	9.97 ± 0.06	3	8.74 ± 0.08	8.60 ± 0.09	1	-1.4	-1.2
R34A	II	plan	8.22 ± 0.07	200	7.38 ± 0.10	7.63 ± 0.04	9	-0.6	-0.8
M35A	II	convex	9.55 ± 0.04	8	7.94 ± 0.07	7.82 ± 0.08	6	-1.7	-1.6
Y36A	II	convex	9.16 ± 0.06	20	7.66 ± 0.11	5.77 ± 0.34	700	-3.4	-1.5
K48A	III	concave	10.36 ± 0.06	1	8.61 ± 0.13	8.37 ± 0.06	2	-2.0	-1.8
Y51A	III	concave	10.29 ± 0.07	2	8.33 ± 0.25	8.38 ± 0.02	2	-1.9	-2.0
R52A	III	concave	10.20 ± 0.03	2	8.35 ± 0.09	7.10 ± 0.07	30	-3.1	-1.8

$\log K_x$ is the log affinity of the toxin for the unoccupied receptor. $\log\alpha.K_x$ is the estimate of the log affinity of the toxins for the NMS-occupied receptor obtained by fitting the inhibition binding curves with the ternary complex equation described in the Materials and Methods section. $\log K_{diss}$ is the log potency of the toxins to inhibit [³H]-NMS dissociation. . Data are mean values ± SEM of at least three independent experiments. $\log\alpha*$ is the estimate of the log cooperativity factor, expressed as $\log K_{diss} - \log K_X$. $\log\alpha^\dagger$ is the estimate of the log cooperativity factor, expressed as $\log \alpha.K_X - \log K_X$

MOL #50773

TABLE 3 : Inhibition potency of wild-type and modified MT7s on the carbamylcholine-induced calcium release on CHO cells expressing the hM_1 receptor.

Modified MT7	$pIC_{50} \pm SEM$	$IC_{50}(mod)/ IC_{50}(wt)$
MT7	8.66 ± 0.10	1
K5A	8.19 ± 0.08	3
S8A	8.21 ± 0.10	3
W10A	8.31 ± 0.08	2
F11A	8.55 ± 0.09	2
Y30A	8.21 ± 0.08	1
S32A	7.98 ± 0.05	5
R34A	7.23 ± 0.03	30
M35A	8.19 ± 0.07	3
Y36A	6.93 ± 0.08	50
K48A	8.35 ± 0.10	2
Y51A	8.52 ± 0.06	1
R52A	7.57 ± 0.02	10

Data are mean values $\pm$ SEM of three independent experiments. The inhibition curves were fitted using a slope factor of 1
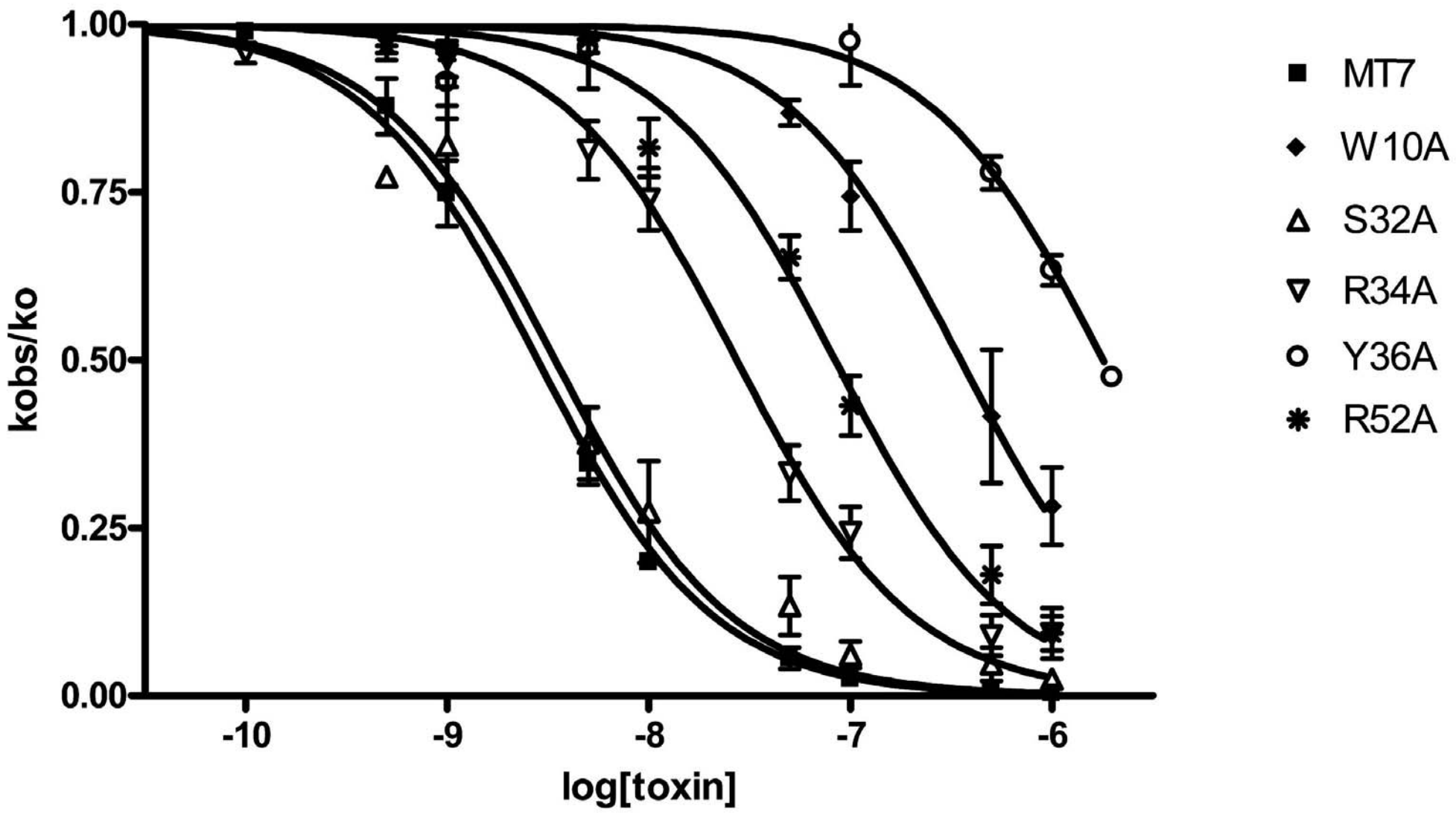
Fig. 1

Fig. 2

Fig. 3

Fig. 4

Legend:
- ■ MT7
- ◆ W10A
- △ S32A
- ▽ R34A
- ○ Y36A
- ✳ R52A

X-axis: log[toxin]
Y-axis: kobs/ko

Fig. 5

Fig. 6

Fig. 7